The International Journal of Advanced Manufacturing Technology (2024) 134:283–296
https://doi.org/10.1007/s00170-024-14100-x

ORIGINAL ARTICLE

Effect of oxygen in shielding gas on weldability in plasma-GMA hybrid welding process of high-tensile strength steel

Quang Ngoc Trinh[1,2] · Shinichi Tashiro[1] · Tetsuo Suga[1] · Hiroto Yamaoka[3] · Kotaro Inose[3] · Kosuke Watanabe[3] · Kengo Hyoma[3] · Yoshihiro Tanabe[3] · Van Hanh Bui[2] · Manabu Tanaka[1]

Received: 1 April 2024 / Accepted: 2 July 2024 / Published online: 19 July 2024

Abstract

This study aims to clarify the effect of oxygen in shielding gas on weldability in the plasma-GMA (Gas Metal Arc) hybrid welding process of high-tensile strength steel plates. The difference in keyhole profile and bead formation, when the GMA shielding gas was pure Ar, Ar + 2% O_2, or Ar + 20% CO_2, was investigated for plate thicknesses of 6 and 9 mm for the first time. It was found that the weld beads were in good condition for 6 mm thickness plates for all shielding gases, which implied that the window of welding conditions for this thickness is wide. In contrast, for 9 mm thickness plates, a fully penetrated weld bead was achieved only in Ar + 20% CO_2, and weld bead penetration in Ar + 20% CO_2 is higher than in pure Ar and Ar + 2% O_2 in the same welding condition. Due to decreased surface tension caused by sufficiently increased oxygen absorbed into the weld pool, the keyhole diameter increased to penetrate the bottom side of the plate, and the depressing weld pool surface under GMA allowed the heat input from the GMA to be directly applied to a deeper position. Consequently, the plasma-GMA hybrid welding process with Ar + 20% CO_2 achieved a complete penetration for a plate of 9 mm thickness, owing to the effects of both phenomena. It proved a potential to increase penetrability in welding thicker plates by controlling oxygen content in shielding gas of GMA adequately.

Keywords Plasma-GMA hybrid welding · Shielding gas · Gas composition · High-tensile strength steel · Plasma keyhole · Oxygen · Surface tension

1 Introduction

The demand for welding thick steel plates is particularly high in the construction, civil engineering machinery, shipbuilding, and railway industry sectors. A typical method for thick plate welding is a multi-layer welding process applying GMA (Gas Metal Arc) welding. However, in this method, it is generally necessary to produce a V or Y groove in the steel plate, and many steps are required to complete the work due to the dramatic increase in the number of welding passes required as the plate thickness increases. Furthermore, the excessive heat input caused by a large number of welding passes coarsens the microstructure of the heat-affected zone, lowering both the tensile strength and absorbed energy of the weld metal [1].

One solution to this problem is applying a hybrid welding process, which has been extensively researched and developed in recent years and is being put to practical use [2, 3]. Plasma-GMA welding, one of the hybrid welding processes, is known to be difficult to control, but it is possible to weld thick steel plates in a single pass with low heat input and deep penetration [4]. In addition, a low-cost square butt joint can be applied to save energy and resources for welding, and the gap tolerance is large. The equipment cost is also much lower than those of other hybrid welding processes, such as laser arc hybrid welding [5].

Plasma arc welding, which involves a very high-temperature constricted arc column, can provide an intensive heat source. The process can be utilized in transferred and

✉ Quang Ngoc Trinh
ngoc.trinhquang@hust.edu.vn

✉ Shinichi Tashiro
tashiro.shinichi.jwri@osaka-u.ac.jp

[1] Joining and Welding Research Institute, Osaka University, Osaka, Japan

[2] School of Mechanical Engineering, Hanoi University of Science and Technology, Hanoi, Vietnam

[3] IHI Corporation, Tokyo, Japan

non-transferred modes, which are useful for generating a deep penetration weld bead [6] and depositing a hard-facing layer on a substrate to increase the hardness and wear resistance [7, 8]. In plasma-GMA hybrid welding, plasma welding is used in the leading position, and a keyhole is formed in the weld pool due to a high arc pressure and a large heat flux brought by the constricted plasma arc, and full penetration until the bottom surface is achieved [9–11]. Then, GMA welding in the trailing position produces metal droplets by melting the welding wire, filling the keyhole and gap with the droplets at a high deposition rate. The shape of this keyhole is determined by the force balance between the arc pressure acting to expand the keyhole and the surface tension of the weld pool acting to contract it [12]. In order to achieve stable welding, it is primarily important to ensure the stability of the keyhole. When the thickness of the base metal increases greatly, the arc pressure from the plasma arc becomes difficult to reach the bottom of the keyhole [13], making stable formation of the keyhole abruptly difficult.

In recent years, cases of plasma-GMA welding of thick steel plates using various welding parameters have been reported. Ishida et al. applied plasma-MIG (Metal Inert Gas) welding using pure Ar gas to plasma welding and GMA welding for high-tensile strength steel with a thickness of 9 mm and a square butt joint [14]. Plasma current and GMA current are direct current and pulse current, respectively. By using a high current of 280 A for plasma welding, although the heat input to the base metal was high, the keyhole was fully penetrated, and welding was achieved. Anh et al. performed plasma-MIG welding on a mild steel plate with a thickness of 12 mm by applying a square butt joint [15]. $Ar + 10\%H_2$ gas was used as the pilot gas for plasma welding. Although the plasma current was a small current of 180 A, the addition of a small amount of hydrogen gas strongly constricted the plasma arc [16], thus increasing the arc pressure and heat flux to the weld pool and improving the penetration ability for the keyhole. However, the effect of added hydrogen on the mechanical properties of the joint has not been evaluated. Skowrońska et al. conducted plasma-MAG (Metal Active Gas) welding using $Ar + 20\%\ CO_2$ to GMA welding for high-tensile strength steel with a thickness of 10 mm applying a Y groove [17]. The plasma current was large at 335 A, and the MAG current was also 360 A or higher. The microstructure and mechanical properties of the joint were also evaluated.

To stabilize plasma-GMA welding of thick steel plates and improve welding quality, it is essential to clarify this processing mechanism and develop a process control technology based on understanding the mechanism.

Since the leading plasma arc and the trailing GMA are arranged close to each other, the electromagnetic force causes arc coupling (interference between the two arcs), causing arc disturbance. As a result, the penetration ability of the plasma arc to the keyhole is impaired, and the heat input position and the transferred position of the droplet in GMA welding largely vary during welding. Ishida et al. investigated the arc coupling mechanism through 3D spectroscopic measurements of plasma temperature and iron vapor concentration fields in plasma-MIG welding [18]. As a result, when a direct current was used for the MIG arc, the plasma arc and the MIG arc were regularly connected, and a direct current path between the two arcs was stably formed. On the other hand, when using a pulsed current, this phenomenon was observed only during the upslope of the pulsed current. Wu et al. observed both arcs in plasma-MIG welding with a high-speed video camera, showing that when a direct current path was formed between the arcs, the MIG current path from the wire to the weld pool was expanded, and droplet detachment was prompted [19]. They then performed a weld pool simulation to evaluate the flow pattern of the weld pool and the driving force to induce the flow [20]. In addition, the transport process of heat and mass provided by droplets in the weld pool was also clarified [21].

Yu et al. tried to control the arc coupling and metal transfer by applying an external magnetic field in plasma-MAG welding [22]. They also investigated the effect of external magnetic field application on the mechanical properties of the joint, presenting the improvement of those [23]. Wang et al. developed high-quality automated welding using plasma-MIG welding [24]. In this research, a multi-vision sensor system was used to image the arc behavior and droplet transfer, and feedback control of welding conditions was carried out based on the information obtained from the images.

In addition to the above, it is considered that the shielding gas composition can also be a controlling factor. The thermodynamic and transport properties of the shielding gas change greatly depending on its composition and strongly affect the temperature field and flow field of the arc [25]. For example, $Ar + 20\%\ CO_2$ is used as a shielding gas in MAG welding. Carbon dioxide has a higher specific heat due to the dissociation reaction, so the arc tends to be more constricted than argon. High arc pressure caused by the constricted arc under the droplet prevents droplet detachment [26]. Consequently, the momentum and heat provided by the arc and droplets to the weld pool are also affected.

On the other hand, it is known that the surface tension of the weld pool decreases, and its temperature dependence changes when the oxygen atoms generated by the dissociation of carbon dioxide are absorbed by the weld pool [27]. AA-TIG (Advanced Active-Tungsten Inert Gas) welding is a welding process that utilizes this temperature-dependent change in surface tension [28]. In this process, the temperature dependence of the surface tension is changed by adding a small amount of oxygen or carbon dioxide to the helium shielding gas. When pure helium shielding gas is used, and

the amount of oxygen in the weld pool can be ignored, the temperature coefficient of surface tension becomes negative, and the Marangoni force is directed from high temperature to low temperature. Therefore, the flow direction on the surface of the weld pool is outward from the center, and the penetration of the weld pool becomes shallow. On the other hand, when 0.4% O_2 is added to helium, the weld pool absorbs a small amount of oxygen, and the temperature coefficient of surface tension becomes positive in the temperature range of the weld pool surface. As a result, the flow on the surface of the weld pool is directed toward the center. Since this causes a downward flow at the center of the weld pool, the penetration of the weld pool becomes deeper. This effect disappears when the amount of oxygen added to helium increases to 4.0%. From the above, plasma-MAG welding, which uses Ar + 20% CO_2 as a shielding gas, is considered to have a different surface tension effect than plasma-MIG welding. However, this effect on the formation of the keyhole and weld bead has not yet been elucidated.

This study aims to clarify the process mechanism of plasma-GMA welding of high-tensile strength steel thick plates for stabilization and sophistication of the welding process. Here, to reduce the heat input to the base metal, the current is set much lower than in other studies [14, 17], and the square butt that does not require machining is used as a desirable condition. As part of this study, for plasma-GMA welding of high-tensile strength steel plate with thicknesses of 6 and 9 mm, the difference in keyhole and bead formation when the shielding gas composition for GMA welding is Ar, Ar + 2% O_2, or Ar + 20% CO_2 is, for the first time, investigated in this paper.

2 Experimental procedure

2.1 Materials

In this study, plasma-GMA hybrid welding was applied to 780 MPa high-tensile strength steel plates (JIS G3128SHY685). The testing specimens were prepared in a square butt joint, including two plates with a dimension of 200 mm in length and 50 mm in width. Two levels of thickness were investigated at 6 and 9 mm. High-strength steel plates used in bridge construction typically range in thickness from 6 to 12 mm. These thicknesses provide structural strength comparable to that of conventional carbon steel plates, which are generally thicker, ranging from 15 to 25 mm [29]. Through screening experiments on the weldability of square groove joints, we determined that thicknesses of 6 and 9 mm are suitable for plasma-GMA hybrid welding in a single pass with three kinds of shielding gas utilized in this study. Additionally, these thickness levels facilitate comprehension of our previous research results [14, 18, 30]. The oxides on the surface of the welding plates were removed by grinding. Tack welding was carried out to maintain a root gap of 1.5 mm. The filler wire used for GMA is JIS Z3312 G78A4 M N5CM3MT, corresponding to AWS A5.28 ER110S-G. The mechanical properties of base metal and filler wire are shown in Table 1, and their chemical compositions are listed in Table 2.

2.2 Experimental conditions

Figure 1 shows a paraxial plasma-GMA hybrid welding experimental setup in the current study. A plasma power source (NW-300ASR, Nippon Steel Welding & Engineering Co., Ltd.) equipped with a plasma arc welding torch (100WH, Nippon Steel Welding & Engineering Co., Ltd.) was combined with a GMA welding system including a welding power source (DP 500, OTC Daihen), a welding torch, and a compatible wire feeder. The plasma power source with a constant current characteristic was operated in EN (Electrode-Negative) mode. In contrast, the GMA welding power source with a constant voltage characteristic was utilized in EP (Electrode-Positive) mode.

An example of an experimental configuration for 9 mm thickness plates is shown in Fig. 1a. A leading plasma torch and trailing GMA welding torch were fixed on a jig to configure a tilt angle of 30° between the two torches. The electrode set-back of the plasma torch was 3 mm. A stand-off of the plasma torch was adjusted at 7 mm and 3 mm for the plate thickness of 6 mm and 9 mm, respectively. The shorter stand-off realizes greater arc pressure and heat flux to the base material, increasing the penetration ability. The distance from the center of the plasma torch to the crossing position of the GMA wire extension on the base metal surface was 15 mm. The contact-tip to workpiece distance (CTWD) was set at 20 mm.

Hybrid welding experiments were carried out with 180 and 220 A plasma welding currents for 6 and 9 mm thicknesses, respectively. Meanwhile, the GMA welding conditions were maintained for both thicknesses. To measure the effect of GMA shielding gas on weld bead formation, three types of shield gas, pure argon, Ar + 2% O_2, and Ar + 20% CO_2, were introduced at 10 L/min. These three kinds of shielding gas were classified into I1, M1, and M2, as described in AWS A5.32, in which Ar + 2% O_2 and Ar + 20%

Table 1 Mechanical properties of base material and filler wire

Materials	Yield point (N/mm^2)	Tensile strength (N/mm^2)	Elongation (%)
Base metal	741	854	18
Filler wire	770	850	18

Table 2 Chemical compositions of base material and filler wire

Chemical composition (wt.%)												
Component	C	Si	Mn	P	S	Cu	Ni	Cr	Mo	V	Ti	CEQ
Base metal	0.09	0.30	1.60	0.012	0.003	0.07	0.003	0.07	0.002	0.01	0.016	0.39
Filler wire	0.09	0.32	1.05	0.008	0.010	–	2.71	0.24	0.49	–	–	–

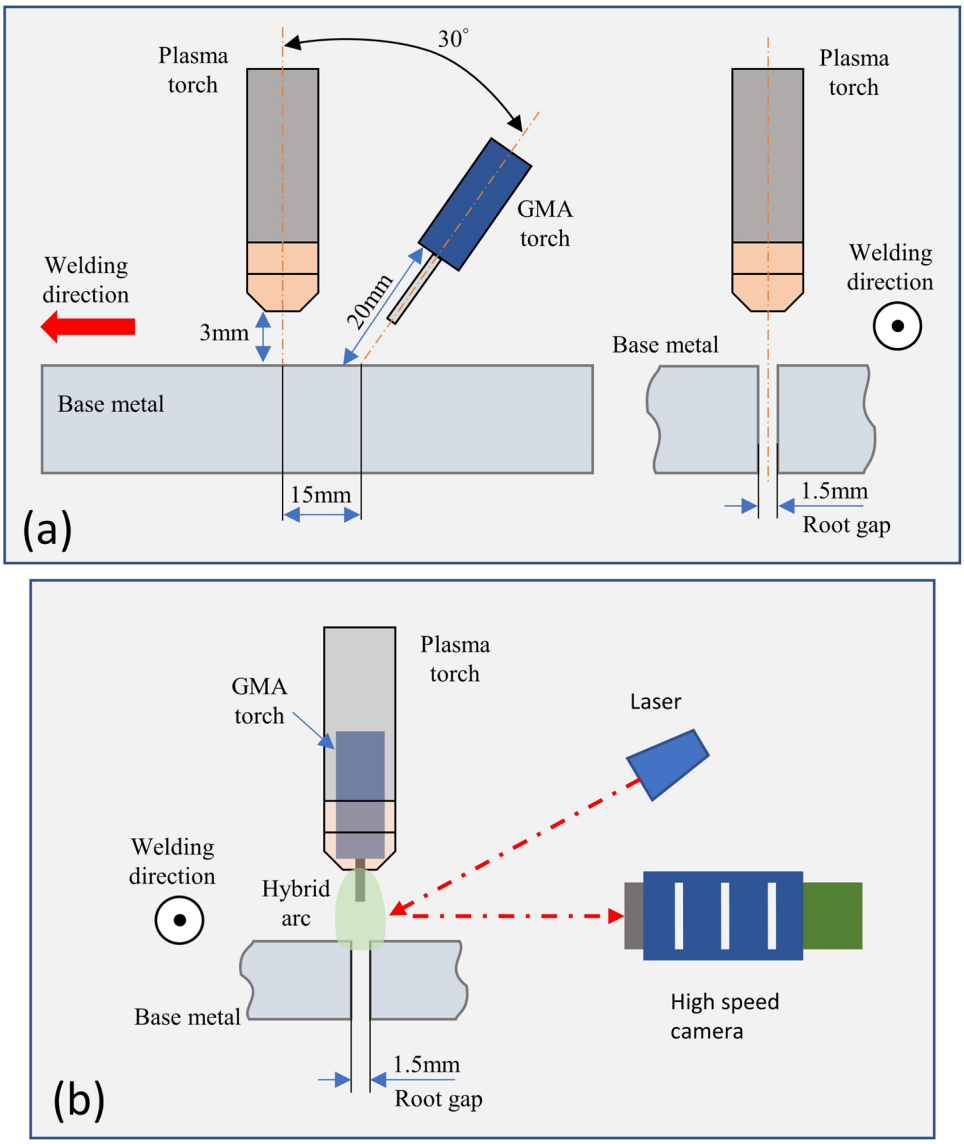

Fig. 1 Experimental setup for **a** hybrid welding and **b** observation system for 9 mm thickness plates

CO_2 were selected in groups M1 and M2, respectively. The other common welding parameters are listed in Table 3.

In order to investigate the metal transfer behavior during the welding process, an observation using a high-speed camera (Memrecam Q1v, Nac Image Technology) combined with a laser illumination system (Cavilux HF, Cavitar) was applied, as shown in Fig. 1b. The camera was equipped with a bandpass filter for a central wavelength equivalent to the laser wavelength at 640 nm, allowing the camera to reduce strong radiation from the arc and capture the reflected laser light simultaneously to visualize the metal transfer process. The camera frame rate and the exposure time were set at 4000 frames per second and 20 µs, respectively. A lens (AF Micro-Nikkor, Nikon) with a focal length and ratio of 105 mm and 1/2.8, respectively, was utilized under f/5.6 of the aperture value to magnify the welding image.

Table 3 Welding parameters

Parameters		Value/unit	
Base metal thickness		**6 mm**	**9 mm**
Plasma welding	Welding current	180 A	220 A
	Stand-off of the torch	7 mm	3 mm
	Shielding gas	Pure Ar; 15 L/min	
	Pilot gas	Pure Ar; 2.5 L/min	
GMA welding	Welding current setting	160 A	
	Wire feeding speed	5.3 m/min	
	Voltage	25 V	
	CTWD	20 mm	
	Wire diameter	1.2 mm	
	Shielding gas	Pure Ar; Ar + 2% O_2; Ar + 20% CO_2; 10 L/min	
Welding travel speed		35 cm/min	40 cm/min
Back shielding gas		None	
Root opening		1.5 mm	

3 Results and discussion

3.1 Weldability of 6 mm thickness plates

Figure 2 shows the weld bead appearances for 6 mm thickness plates under three types of GMA shielding gas. The welding was performed in approximately 140 mm length, and the top and bottom view photos are presented. It can be observed that a good weld bead can be obtained under all three shielding gases. A red dashed line on the images of the bottom side indicates the position to investigate the cross section of weld beads.

Figure 3 shows the cross section in the three shielding gas conditions for plates with a 6 mm thickness. The macro photos indicate that the weld bead of hybrid welding contains two weld metal regions. The solidification of the melted filler wire from GMA welding contributed to the upper weld metal region. Meanwhile, plasma arc welding mainly produced the lower weld metal region from the molten base material. In Fig. 3a, it can be observed that the weld bead with pure Ar shielding gas presented a round

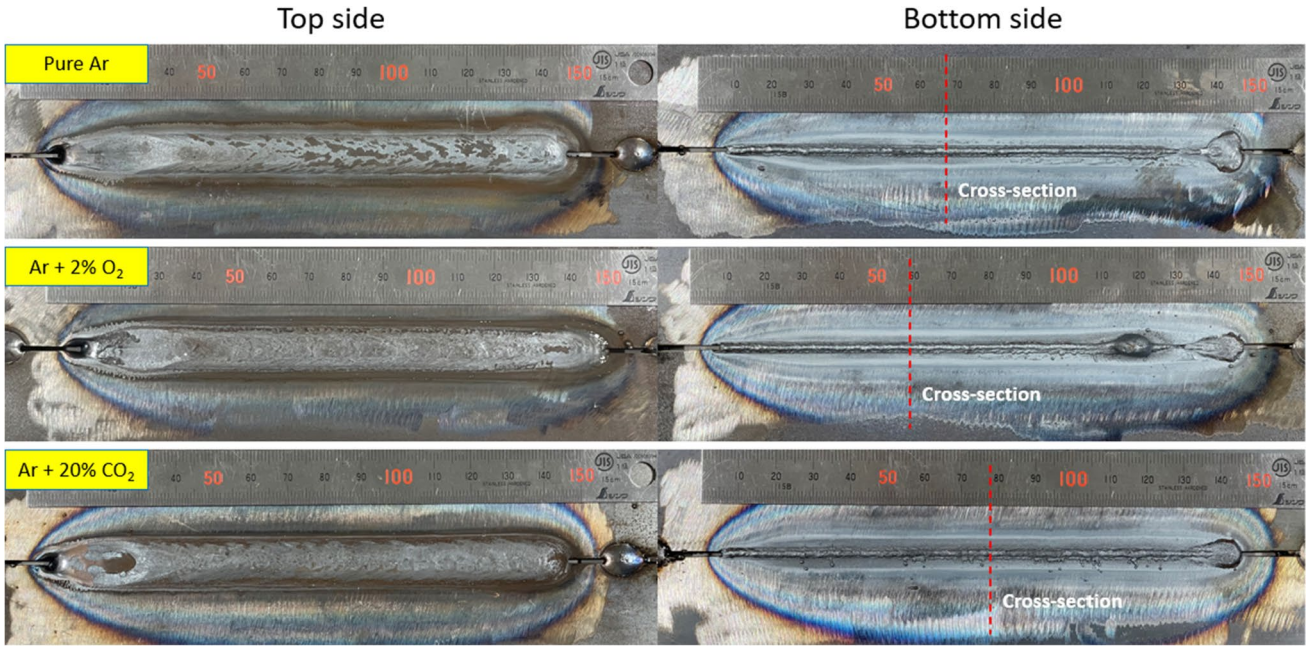

Fig. 2 Weld bead appearance for 6 mm thickness plates in **a** pure Ar, **b** Ar + 2% O_2, and **c** Ar + 20% CO_2 shielding gas

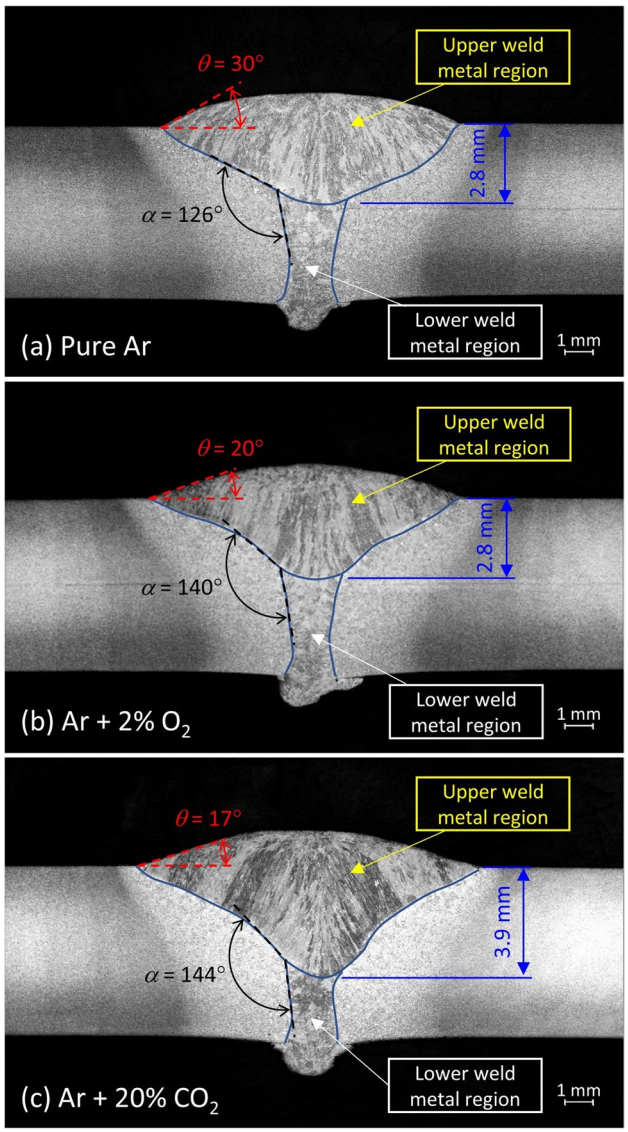

Fig. 3 Weld bead cross section of 6 mm thickness plates in **a** pure Ar, **b** Ar + 2% O_2, and **c**)Ar + 20% CO_2 shielding gas

shape of the upper part, in which the convexity angle (flank angle θ) at the weld toe was 30°. The angle at the transition location between the upper and lower weld metal regions (transition angle α) was 126°. The flank angle significantly decreased to 20° when Ar + 2% O_2 was used and then to 17° with Ar + 20% CO_2 shielding gas, as predicted in Fig. 3b, c. Reduction of flank angle was thought to diminish the stress concentration phenomenon and enhance the fatigue strength of weld joints [31–33]. Furthermore, the transition angle was increased from 126 to 140° and 144° when 2% O_2 and 20% CO_2 were included in the shielding gas, respectively. This result indicated that the molten metal became more fluid when 20% CO_2 was added compared to 2% of O_2 and to pure Ar shielding gas. In addition, the penetration of GMA welding in pure Ar and Ar + 2% O_2 is similar at 2.8 mm, which is less than in Ar + 20% CO_2 at 3.9 mm.

Figure 4 shows the arc appearance and metal transfer behavior for 6 mm thickness plates in three shielding gases. The figure shows one transfer cycle within 8 ms for each condition. Although the GMA welding parameters were maintained during all the experiments, the transfer achieved one pulse and one droplet independently of shielding gas types. However, the arc length in Ar + 20% CO_2 was observed to be less than that in pure Ar and Ar + 2% O_2 circumstances. It can be considered that the arc in Ar + 20% CO_2 becomes slightly constricted due to a high specific heat of CO_2 [34]. When the specific heat is high, the arc contracts, reducing the cross-sectional area of the arc, which results in a larger voltage drop across the arc. Therefore, the arc length becomes shorter under the constant voltage characteristic. On the other hand, the arc was thought to extend upward to the contact tip in the other argon-rich gases because of the separation into metal vapor plasma and shielding gas plasma in GMA plasma, which was reported in many studies in pure Ar GMA welding [35].

3.2 Weldability of 9 mm thickness plates

Figure 5 presents the weld bead appearances for 9 mm thickness plates. The same weld bead length of 140 mm was produced also for this thickness. From the bottom side, it was observed that the weld beads in pure Ar and Ar + 2% O_2 gases had insufficient penetration. A weld bead with full penetration was obtained only in Ar + 20% CO_2 gas, as shown in Fig. 5c. In addition, the position for investigation of a cross section of the keyhole and weld bead was indicated by dashed blue and red lines, respectively.

Figure 6 depicts the weld bead cross section for 9 mm thickness plates. The macro photos show incomplete root penetration for weld beads in pure Ar and Ar + 2% O2, as shown in Fig. 6a, b. On the other hand, a good bead with full penetration was achieved in Ar + 20% CO_2 in Fig. 6c. The weld beads show two solidification regions, similar to those for 6 mm thickness plates in Fig. 3. The weld metal provided by the GMA welding in Fig. 6a almost resembled that in Fig. 6b. In both cases, the lower part of the gap was not melted by the plasma arc to be the leading heat source, so the weld metal by GMA welding formed high reinforcement above the base metal surface. The heat input was thought to be the same due to maintaining welding conditions, but the increase in the weld pool size and depression of the weld pool surface led to an improvement in flowing molten metal downward.

On the contrary, in Fig. 6c, the gap's lower part was melted and filled with weld metal at all heights. The lack of penetration in weld beads was thought to be related to the plasma arc energy, which can be considered from the

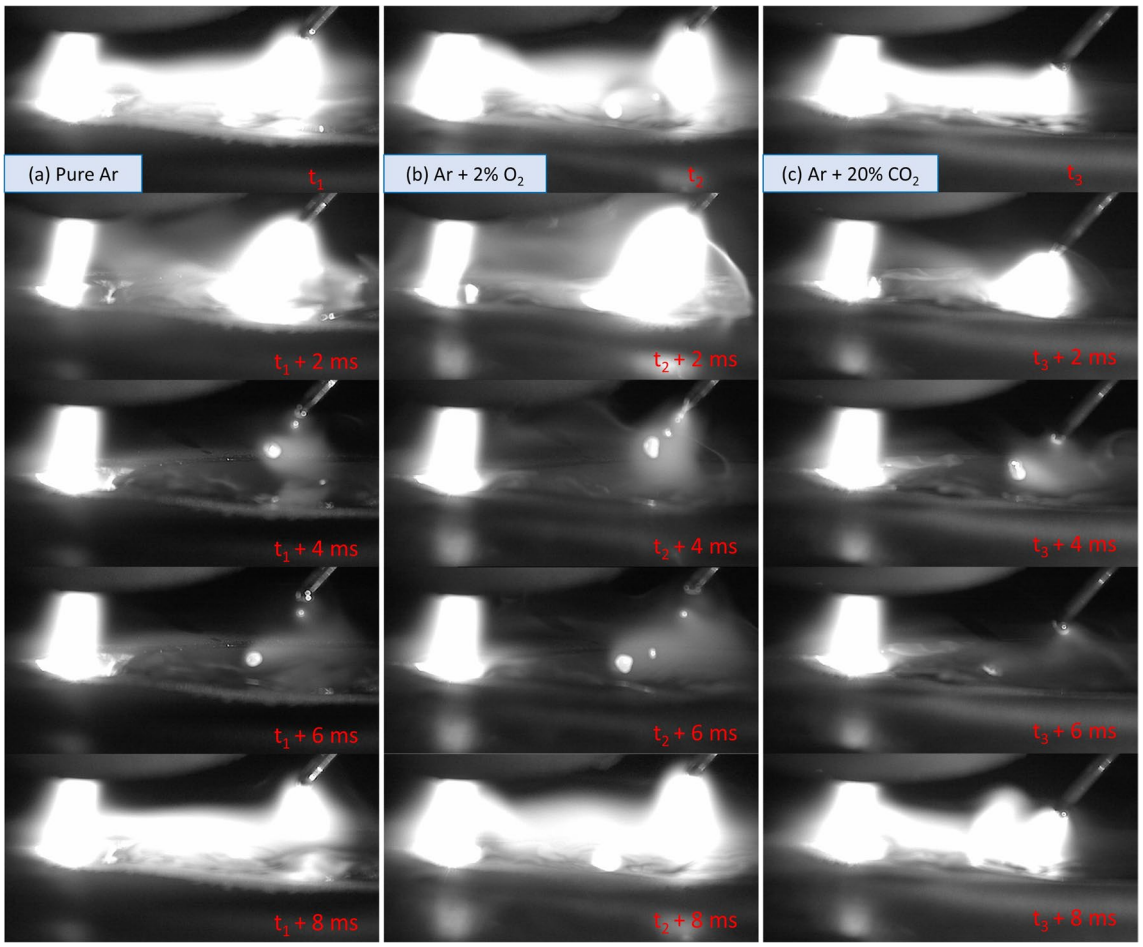

Fig. 4 Arc appearance and metal transfer behavior for 6 mm thickness plates in **a** pure Ar, **b** Ar + 2% O_2, and **c** Ar + 20% CO_2 shielding gas

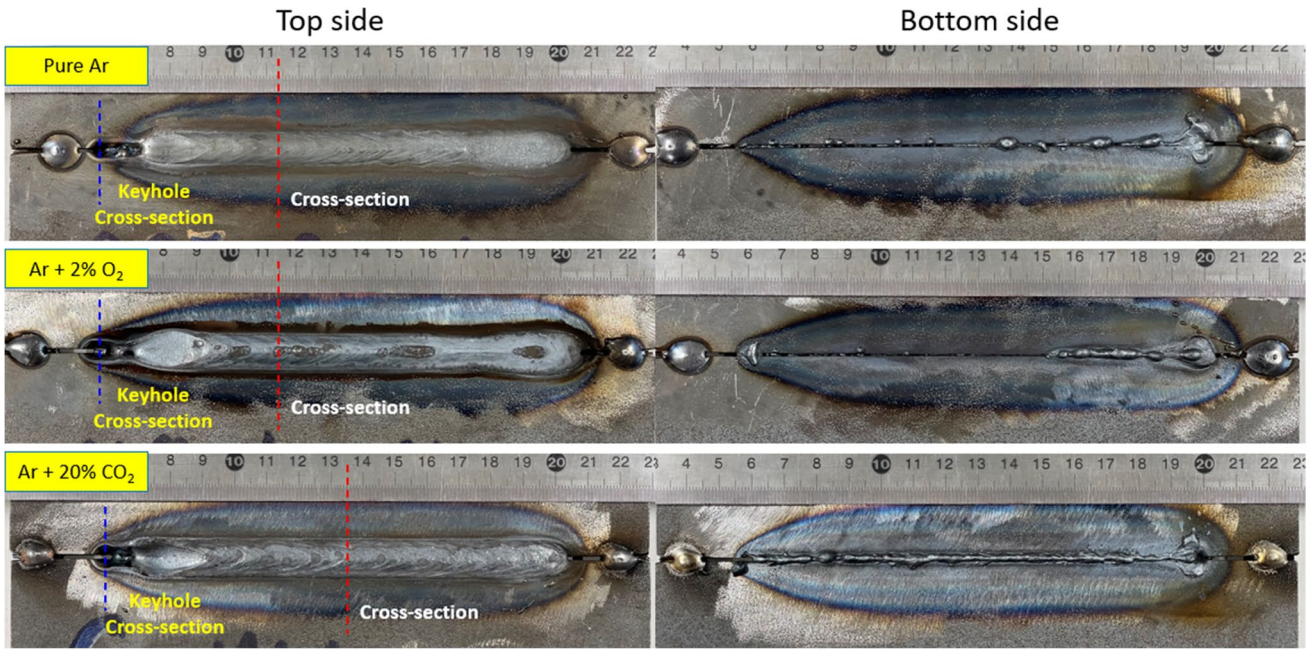

Fig. 5 Weld bead appearance for 9 mm thickness plates in **a** pure Ar, **b** Ar + 2% O_2, and **c** Ar + 20% CO_2 shielding gas

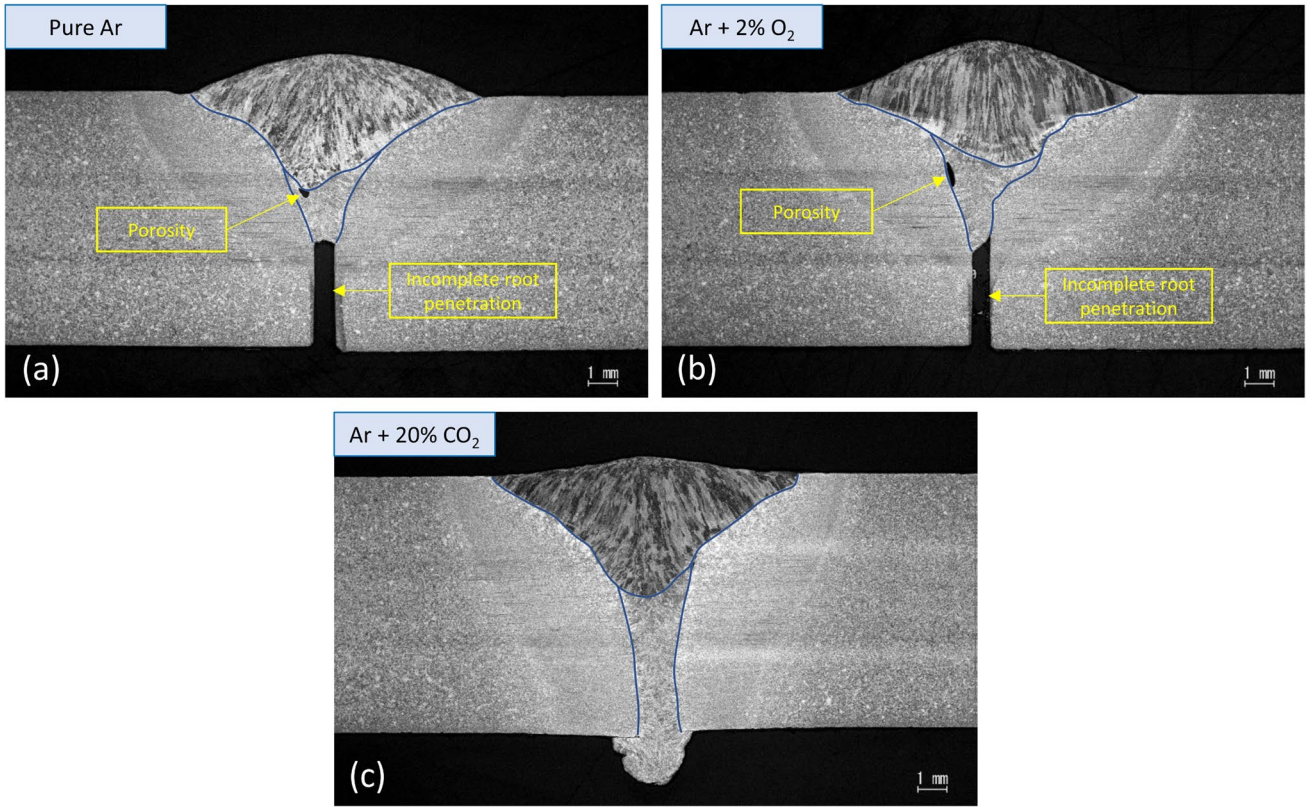

Fig. 6 Weld bead cross section for 9 mm thickness plates in **a** pure Ar, **b** Ar + 2% O_2, and **c** Ar + 20% CO_2 shielding gas

keyhole behavior during welding. To clarify the difference in weld bead formation, cross sections of the plasma keyhole were investigated.

Figure 7 presents the plasma's keyhole geometry of the weld beads in three shielding gases. The keyhole diameters at the top surface of the plates in pure Ar, Ar + 2% O_2, and Ar + 20% CO_2 were 5.48, 6.27, and 7.67 mm, respectively. In addition, the keyhole profiles were compared in Fig. 7d. It can be observed that the width of the keyhole increased when the shielding gas changed from pure Ar to Ar + 2% O_2 and then to Ar + 20% CO_2. The results indicate that the keyhole broadened with increasing oxygen content in the shielding gas. Furthermore, it was also found that the base metal surface inside the gap around the bottom surface was not melted except for the case in Ar + 20% CO_2.

Figure 8 shows arc appearance and metal transfer behavior for 9 mm thickness plates during a cycle time of 8 ms. The time step for each condition is 2 ms. During this time, one droplet was transferred to the weld pool. For instance, in Fig. 8a, the first image shows the moment of the initial interaction between the plasma arc and GMA in pure Ar at t_1. At $t_1 + 2$ ms, the GMA current reached the peak current, and a droplet was detached from the wire. The droplet can be observed at $t_1 + 4$ and $t_1 + 6$ ms, which refers to the base current time. This phenomenon was reported by Ishida et al. [18], who found that the arc coupling between the plasma arc and GMA was significant during the upslope phase of the peak current period. The metal transfer behavior in Ar + 2% O_2 was similar to that in pure Ar.

Meanwhile, the arc length of GMA welding in Ar + 20% CO_2 is smaller than that in pure Ar and Ar + 2% O_2. In addition, the weld pool surface was largely depressed under the top surface of the base metal behind the keyhole, as observed in Fig. 8c. It was considered to be caused by the greater arc pressure and heat flux given by the plasma arc with the shorter stand-off, higher current, and faster welding velocity compared with those for a thickness of 6 mm. It was also seen that part of the droplets was directly transferred to the deep portion of the keyhole due to this depression.

3.3 Mechanism of the GMA welding shielding gas effect

From the experimental results, the mechanism of the GMA shielding gas effect on the difference in weld bead formation was suggested. The arc lengths of the GMA welding in pure Ar for plates of 6 and 9 mm thickness were compared in Fig. 9. In Fig. 9a, b, an image for the moment t_0 at 0.25 ms before the arc coupling and another image for the moment of the arc coupling ($t_0 + 0.25$ ms) were presented for

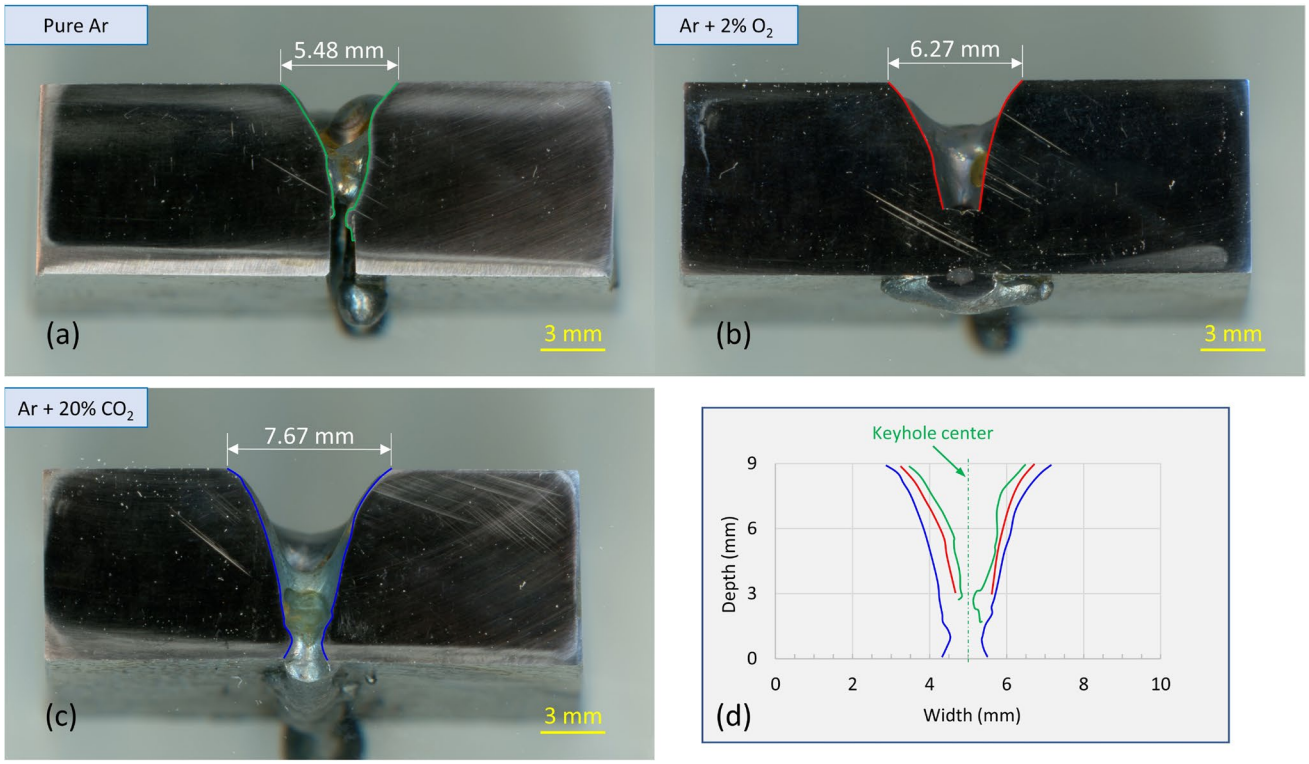

Fig. 7 Keyhole cross section for 9 mm thickness plates in **a** pure Ar, **b** Ar + 2% O_2, and **c** Ar + 20% CO_2 shielding gas

6 mm thickness plates, respectively. The similarity of the arc coupling phenomenon for the 9 mm thickness plates is also depicted in Fig. 9c, d. It was observed that the arc length was kept at 6.5 mm for two different thicknesses because GMA welding conditions were maintained.

Figure 10 shows the arc lengths of the GMA welding in Ar + 20% CO_2 for plates of 6 and 9 mm thickness. In Fig. 10a, the time t_3 indicated a moment of 0.25 ms before arc coupling occurred. The plasma arc and GMA interfered at t_3 + 0.25 ms, as shown in Fig. 10b. The arc length from the wire tip to the weld pool surface was 4.3 mm for 6 mm thickness plates. Due to the maintained GMA welding condition, the arc length in Ar + 20% CO_2 was thought to be preserved when the thickness of the plate increased from 6 to 9 mm, similar to that for pure Ar shown in Fig. 9. Thus, both arc lengths in Fig. 10c, d were considered 4.3 mm, implying that the weld pool surface was depressed under the top surface for 9 mm thickness plates in Ar + 20% CO_2.

The microstructure and mechanical properties of 780 MPa high-strength steel in laser-GMA hybrid welding were observed by Suga et al. [30]. The investigation compared the weldability of a one-layer-one-pass weld bead under the effect of filler wire characteristics and GMA shielding gas composition. Three kinds of shielding gas similar to the current study were examined. They reported that Ar + 20% CO_2 was beneficial for reducing spatter, while Ar + 2% O_2 resulted in the highest spatter level. The effect of filler wire type on microstructure was measured to have no significant difference. Regarding the effect of shielding gas on microstructure and mechanical properties, the Ar + 20% CO_2 showed a lower hardness and corresponding tensile strength compared to Ar + 2% O_2 and pure Ar, but the highest absorbed energy for a 590 MPa filler wire, which is a lower grade than the filler wire in this study. On the other hand, the hardness of the different sheet thicknesses was observed to be almost consistent. We believe that the effect of shielding gas on the microstructure was similar to the previous study. The conceptualization of this study focuses on the weldability and weld bead formation of plasma-GMA hybrid welding. We propose that future research should include additional experiments to build upon our current findings, aiming to provide a more comprehensive understanding of the mechanical properties and microstructure of weld beads produced by plasma-GMA hybrid welding under varying welding conditions.

Figure 11 presents a schematic of welding behavior in pure Ar and Ar + 20% CO_2 for 9 mm thickness plates at the arc coupling moment. The weld pool is small, and the weld bead is incomplete in the weld penetration for pure Ar in Fig. 11a. It was considered that in pure Ar, the molten metal had a high surface tension due to negligibly small oxygen content. On the other hand, in Ar + 20% CO_2, a large

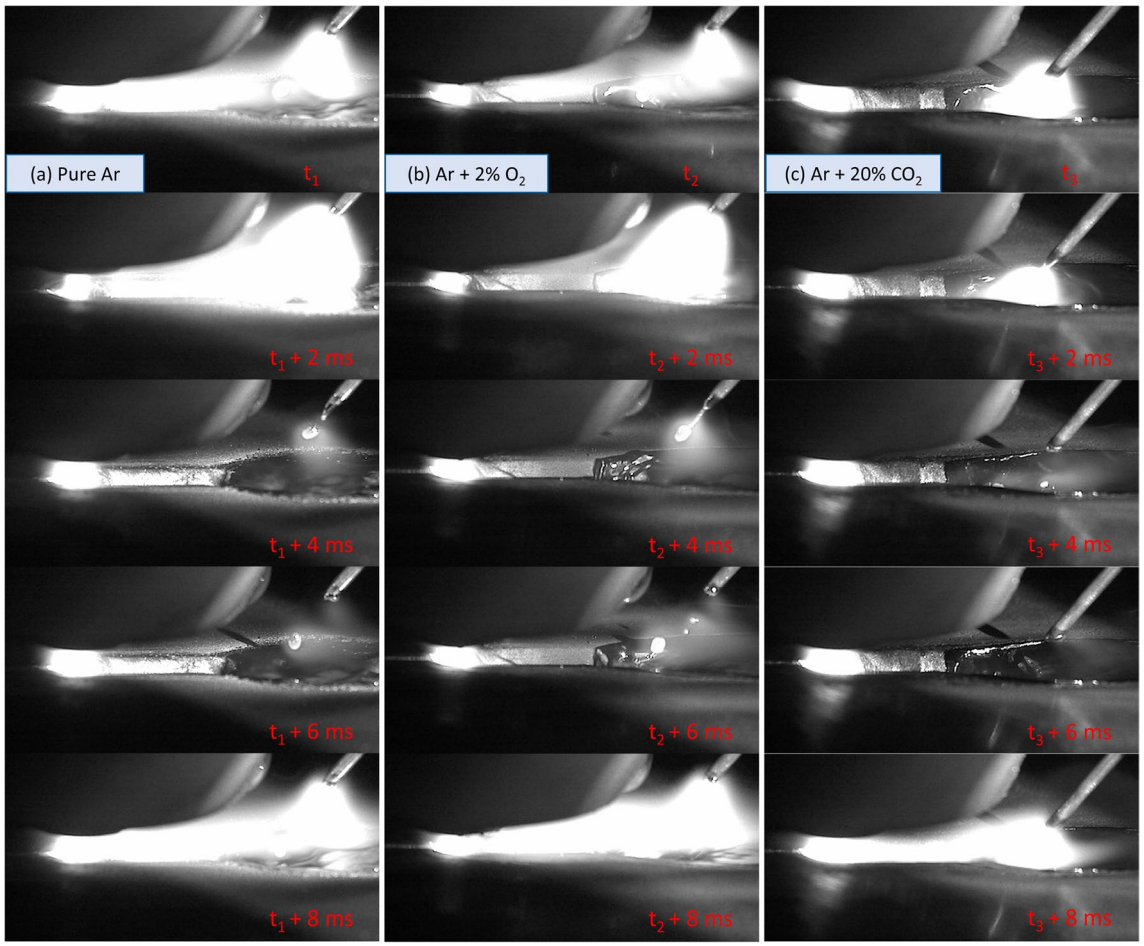

Fig. 8 Arc appearance and metal transfer behavior for 9 mm thickness plates in **a** pure Ar, **b** Ar + 2% O_2, and **c** Ar + 20% CO_2 shielding gas

weld pool and a full penetration bead were obtained, as presented in Fig. 11b. In this case, the weld pool, especially at the GMA area, was thought to absorb much oxygen in the shielding gas, which is then transported frontward by weld pool convection [27, 36].

Many studies reported that the surface tension of a liquid metal depends on the temperature and oxygen content in the liquid [27, 36]. It should be noted that the surface tension is thought to decrease with increasing temperatures and oxygen content in the range for this experiment. The keyhole profile is governed mainly by the force balance between plasma arc pressure and surface tension. As a result, the keyhole diameter increased to penetrate the bottom side of the plate due to the sufficient presence of oxygen. By expanding the keyhole diameter on the bottom side, the heat input by the plasma arc can be given to the deeper region, contributing to the melting of the bottom side metal. In addition, this expansion increases the amount of plasma flow outflowing below through the keyhole exit, inducing downward weld pool flow near the keyhole surface due to plasma shear force. This weld pool flow might transport energy to the bottom side, also contributing to the penetration [6]. Furthermore, reducing surface tension also has the effect of depressing the surface of the weld pool below the GMA welding, allowing the heat input from the GMA to be directly applied to a deeper position. Consequently, plasma-GMA with Ar + 20% CO_2 can achieve complete penetration even with a plate thickness of 9 mm, owing to the effects of both phenomena.

Recently, the rationalization of steel bridge fabrication in both design and execution has been strongly demanded to save energy and reduce initial construction costs. High-tensile strength steel plates are widely used to reduce the thickness and weight of components [37, 38]. Additionally, achieving full penetration welds in a single pass can minimize distortion and enhance production efficiency. Plasma-GMA hybrid welding is a promising process capable of welding thick plates in one pass with high-concentration heat input and deep penetration. This study investigates the application of plasma-GMA hybrid welding to a 9 mm thick square groove joint of high-strength steel, which offers a cost-effective alternative to the more complex V or Y groove weld joints [17].

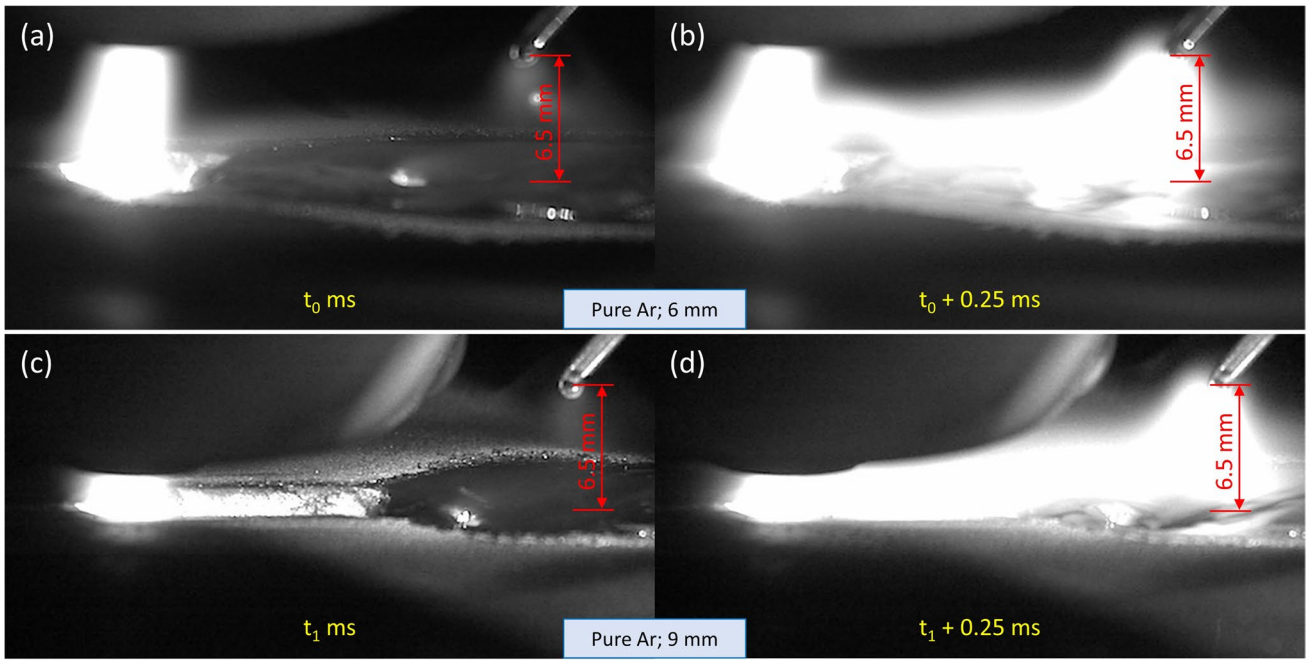

Fig. 9 Comparison of arc length in pure Ar shielding gas for 6 and 9 mm thickness plates

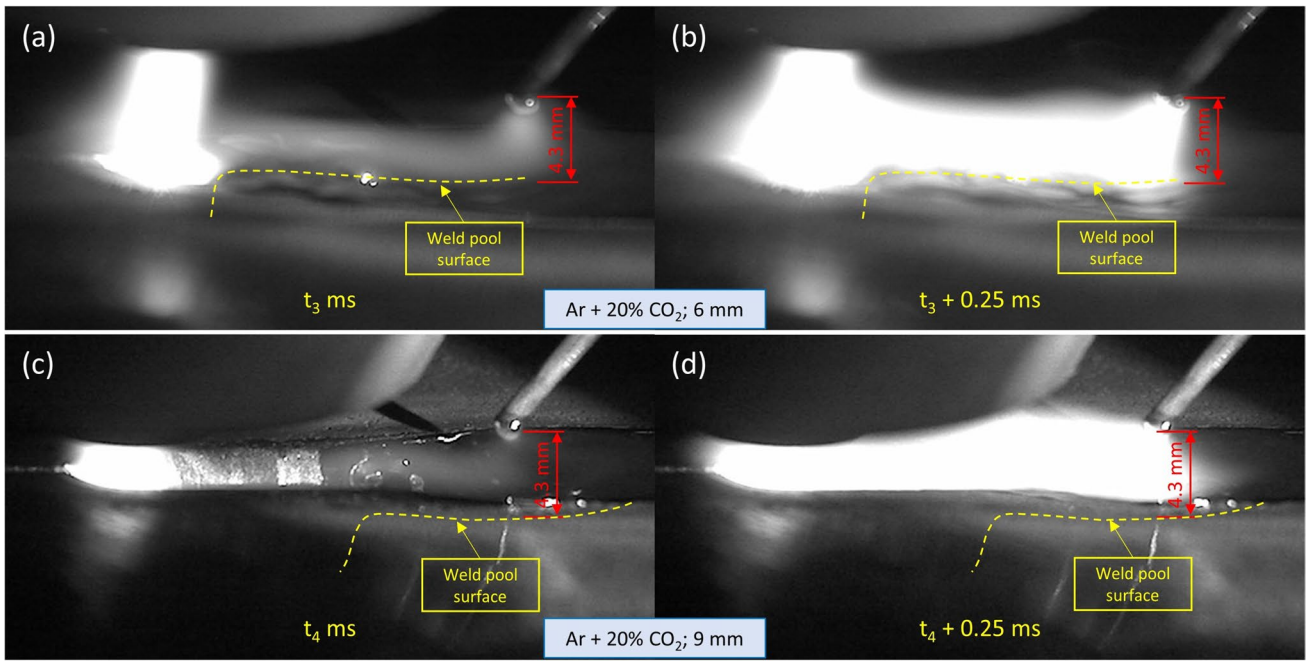

Fig. 10 Comparison of arc length in Ar + 20% CO_2 shielding gas for 6 and 9 mm thickness plates

Our findings indicate that plasma-GMA hybrid welding is significantly improved when using Ar + 20% CO_2 as the shielding gas. This approach provides two major advantages: deep penetration at the top side, resulting in a regular weld bead shape, and achieving full penetration due to the decreased surface tension of the weld pool at the plasma side. It has been demonstrated that controlling the oxygen content in the shielding gas can enhance penetration in welding thicker plates. Furthermore, improving the

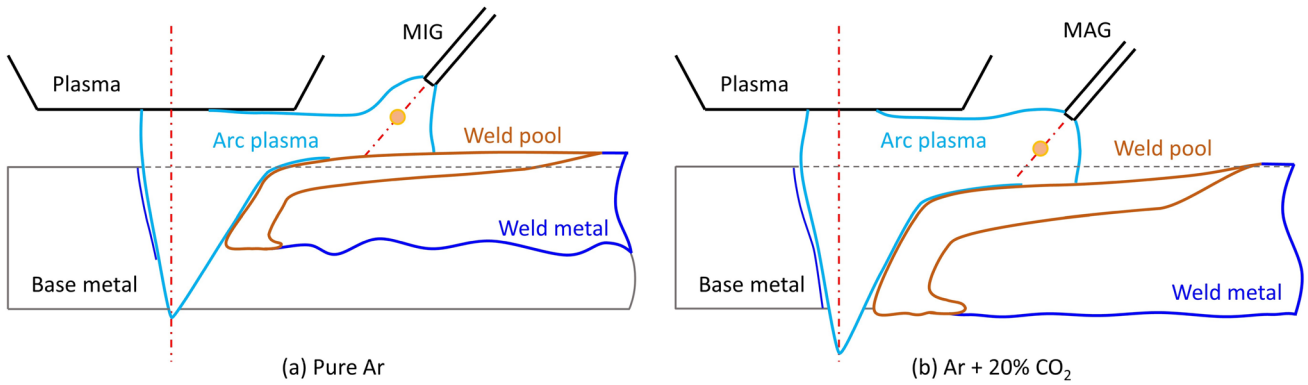

Fig. 11 Schematic of the effect of shielding gas on welding behavior in plasma-GMA hybrid welding for a 9 mm thickness plate

weldability of thick plates at lower plasma welding currents can save energy and reduce welding process costs.

4 Conclusion

This study measured the effect of GMA shielding gas in plasma-GMA hybrid welding on the weld bead formation. Three shielding gases, including pure Ar, Ar + 2% O_2, and Ar + 20% CO_2, were applied for a high-tensile strength steel 780 MPa grade with 6 and 9 mm thicknesses. From the comparison, the main conclusions are summarized as follows:

1. In welding 6 mm thickness plates, the weld beads are acceptable for all shielding gas compositions, which implies that the window for welding conditions for this thickness is wide.
2. In welding 9 mm thickness plates, a good weld bead can be achieved only in Ar + 20% CO_2, and weld bead penetration in Ar + 20% CO_2 is higher than in pure Ar and Ar + 2% O_2 for the same welding condition.
3. In Ar + 20% CO_2, the keyhole diameter was increased, and the GMA weld pool surface was depressed due to a decrease in surface tension of the weld pool caused by the increased oxygen contents, which supported more heat transfer to the bottom side of the base metal to increase weld bead penetration.

The result demonstrates that plasma-GMA hybrid welding, using Ar + 20% CO_2 as shielding gas, effectively welds 9 mm thick high-strength steel plates in a single pass, offering cost and energy savings. This method provides deep penetration and regular weld bead shapes, enhancing production efficiency. Controlling the oxygen content in the shielding gas is crucial for improving weld penetration and weldability of thicker plates.

Acknowledgements The authors are grateful for the support this study received through a joint research agreement between the Joining and Welding Research Institute, Osaka University, Japan; School of Mechanical Engineering, Hanoi University of Science and Technology, Hanoi, Vietnam; IHI Corporation, Tokyo, Japan; and IHI Infrastructure Asia Co., Ltd., Haiphong, Vietnam.

Author contribution Ngoc Quang Trinh: investigation, visualization, writing–original draft preparation. Shinichi Tashiro: conceptualization, writing–review and editing. Tetsuo Suga: project administration. Hiroto Yamaoka: resources, validation. Koutarou Inose: resources, validation. Kosuke Watanabe: resources, validation. Kengo Hyoma: resources, validation. Yoshihiro Tanabe: resources, validation. Hanh Van Bui: validation. Manabu Tanaka: validation, supervision.

Funding Open Access funding provided by Osaka University. This work was supported by JSPS KAKENHI (Grant Number JP21K04710), the Project on Design & Engineering by Joint Inverse Innovation for Materials Architecture (DEJI2MA) from the Ministry of Education, Culture, Sports, Science and Technology (MEXT), and an OU Master Plan Implementation Project promoted under Osaka University.

Declarations

Ethics approval The authors state that the present work is in compliance with the ethical standards.

Consent to participate All the authors listed have approved the manuscript and consented to participate.

Consent for publication All the authors listed have approved the manuscript and consented for publication.

Conflict of interest The authors declare no competing interests.

References

1. Kou S (2003) Welding metallurgy, 2nd edn. John Wiley & Sons Inc, New Jersey
2. Bagger C, Olsen FO (2005) Review of laser hybrid welding. J Laser Appl 17:2–14. https://doi.org/10.2351/1.1848532
3. Li Z, Srivatsan TS, Li Y, Zhang W (2013) Coupling of laser with plasma arc to facilitate hybrid welding of metallic materials: a review. J Mater Eng Perform 22:384–395. https://doi.org/10.1007/s11665-012-0280-6
4. Pilat Z, Szulc J (2014) Concept of the model robotized cell for plasma-GMAW hybrid welding. Appl Mech Mater 613:43–52. https://doi.org/10.4028/www.scientific.net/AMM.613.43
5. Bunaziv I, Akselsen OM, Frostevarg J, Kaplan AFH (2018) Laser-arc hybrid welding of thick HSLA steel. J Mater Process Technol 259:75–87. https://doi.org/10.1016/j.jmatprotec.2018.04.019
6. Tashiro S (2024) Interaction mechanism of arc, keyhole, and weld pool in keyhole plasma arc welding: a review. Materials 17:1348. https://doi.org/10.3390/ma17061348
7. Kalyankar V, Bhoskar A, Deshmukh D, Patil S (2022) On the performance of metallurgical behaviour of Stellite 6 cladding deposited on SS316L substrate with PTAW process. Can Metall Q 61:130–144. https://doi.org/10.1080/00084433.2022.2031681
8. Bhoskar A, Kalyankar V (2024) Effect of powder feed rate on the structure and properties of plasma deposited Stellite 6 cladding on SS316L stainless steel substrate. Met Sci Heat Treat 65:691–697. https://doi.org/10.1007/s11041-024-00991-w
9. Wu CS, Wang L, Ren WJ, Zhang XY (2014) Plasma arc welding: process, sensing, control and modeling. J Manuf Process 16:74–85. https://doi.org/10.1016/j.jmapro.2013.06.004
10. Liu ZM, Cui SL, Luo Z et al (2016) Plasma arc welding: process variants and its recent developments of sensing, controlling and modeling. J Manuf Process 23:315–327. https://doi.org/10.1016/j.jmapro.2016.04.004
11. Jiang F, Li W, Xu B et al (2024) Variable polarity plasma arc welding: process development and its recent developments of detecting, modeling, and controlling. J Manuf Process 114:1–17. https://doi.org/10.1016/j.jmapro.2024.01.078
12. Wu D, Van Nguyen A, Tashiro S et al (2019) Elucidation of the weld pool convection and keyhole formation mechanism in the keyhole plasma arc welding. Int J Heat Mass Transf 131:920–931. https://doi.org/10.1016/j.ijheatmasstransfer.2018.11.108
13. Xu B, Jiang F, Chen S, et al (2018) Numerical analysis of plasma arc physical characteristics under additional constraint of keyhole. Chinese Physics B 27: https://doi.org/10.1088/1674-1056/27/3/034701
14. Ishida K, Tashiro S, Mizutani M, Tanaka M (2021) Study on the weld bead formation on square-groove butt joint using plasma-MIG hybrid welding process. Yosetsu Gakkai Ronbunshu/Quarterly J Japan Weld Soc 38:135S-138S. https://doi.org/10.2207/QJJWS.38.135S
15. Van Anh N, Tashiro S, Van Hanh B, Tanaka M (2017) Development of plasma-MIG hybrid welding process. Yosetsu Gakkai Ronbunshu/Quarterly J Japan Weld Soc 35:132S-136S. https://doi.org/10.2207/QJJWS.35.132S
16. Murphy AB, Tanaka M, Tashiro S, et al (2009) A computational investigation of the effectiveness of different shielding gas mixtures for arc welding. J Phys D Appl Phys 42: https://doi.org/10.1088/0022-3727/42/11/115205
17. Skowronska B, Chmielewski T, Golanski D, Szulc J (2020) Weldability of S700MC steel welded with the hybrid plasma + MAG method. Manuf Rev (Les Ulis) 7: https://doi.org/10.1051/mfreview/2020001
18. Ishida K, Tashiro S, Nomura K et al (2022) Elucidation of arc coupling mechanism in plasma-MIG hybrid welding process through spectroscopic measurement of 3D distributions of plasma temperature and iron vapor concentration. J Manuf Process 77:743–753. https://doi.org/10.1016/j.jmapro.2022.04.002
19 Wu D, Tashiro S, Wu Z et al (2020) Interactive phenomena in hybrid KPAW–GMAW-P. Weld J 99:146s–155s. https://doi.org/10.29391/2020.99.014
20. Wu D, Tashiro S, Wu Z et al (2020) Analysis of heat transfer and material flow in hybrid KPAW-GMAW process based on the novel three dimensional CFD simulation. Int J Heat Mass Transf 147:118921. https://doi.org/10.1016/j.ijheatmasstransfer.2019.118921
21. Wu D, Ishida K, Tashiro S et al (2023) Dynamic keyhole behaviors and element mixing in paraxial hybrid plasma-MIG welding with a gap. Int J Heat Mass Transf 200:123551. https://doi.org/10.1016/j.ijheatmasstransfer.2022.123551
22. Yu J, Wang B, Zhang H et al (2020) Characteristics of magnetic field assisting plasma GMAW-P. Weld J 99:25s–38s. https://doi.org/10.29391/2020.99.003
23. Yu J, Zhang H, He P et al (2021) Arc characteristics and welding process of magnetic field assisting plasma-GMAW-P. Weld J 100:1–12. https://doi.org/10.29391/2021.100.001
24. Wang W, Yamane S, Wang Q et al (2023) Visual sensing and quality control in plasma MIG welding. J Manuf Process 86:163–176. https://doi.org/10.1016/j.jmapro.2022.12.041
25. Murphy AB, Arundelli CJ (1994) Transport coefficients of argon, nitrogen, oxygen, argon-nitrogen, and argon-oxygen plasmas. Plasma Chem Plasma Process 14:451–490. https://doi.org/10.1007/BF01570207
26. Tashiro S, Murphy AB, Tanaka M (2018) Numerical simulation of fume formation process in GMA welding. Weld World 62:1331–1339. https://doi.org/10.1007/s40194-018-0656-9
27. DebRoy T, David SA (1995) Physical processes in fusion welding. Rev Mod Phys 67:85–112. https://doi.org/10.1103/RevModPhys.67.85
28. Fujii H, Sato T, Lu S, Nogi K (2008) Development of an advanced A-TIG (AA-TIG) welding method by control of Marangoni convection. Mater Sci Eng, A 495:296–303. https://doi.org/10.1016/j.msea.2007.10.116
29. Wright WJ (2015) Steel bridge design handbook: bridge steels and their mechanical properties. In: FHWA-HIF-16–002 . United States. Federal Highway Administration. Office of Bridges and Structures
30. Suga T, Murai Y, Kobashi T et al (2012) Research on laser-arc hybrid welding of Ht780 steel. Weld World 56:105–118. https://doi.org/10.1007/BF03321401
31. Teng T-L, Fung C-P, Chang P-H (2002) Effect of weld geometry and residual stresses on fatigue in butt-welded joints. Int J Press Vessels Pip 79:467–482. https://doi.org/10.1016/S0308-0161(02)00060-1
32. Ishigami A, Roy MJ, Walsh JN, Withers PJ (2017) The effect of the weld fusion zone shape on residual stress in submerged arc welding. Int J Adv Manuf Technol 90:3451–3464. https://doi.org/10.1007/s00170-016-9542-z
33. Hwang I, Kim DY, Jeong G, et al (2017) Effect of weld bead shape on the fatigue behavior of GMAW lap fillet joint in GA 590 MPa steel sheets. Metals (Basel) 7: https://doi.org/10.3390/met7100399

34. de Resende AA, Keocheguerians F, Vilarinho LO (2010) The influence of CO_2 and O_2 content on globular spray transition current when using argon-based blends in GMAW of ER 70s 6 wire. Weld Int 24:593–601. https://doi.org/10.1080/09507110903568828
35. Schnick M, Füssel U, Hertel M, et al (2010) Metal vapour causes a central minimum in arc temperature in gas-metal arc welding through increased radiative emission. J Phys D Appl Phys 43: https://doi.org/10.1088/0022-3727/43/2/022001
36. Sahoo P, Debroy T, McNallan MJ (1988) Surface tension of binary metal-surface active solute systems under conditions relevant to welding metallurgy. Metall Trans B 19:483–491. https://doi.org/10.1007/BF02657748
37. Skoglund O, Leander J, Karoumi R (2020) Overview of steel bridges containing high strength steel. Int J Steel Struct 20:1294–1301. https://doi.org/10.1007/s13296-020-00360-2
38. Tümer M, Schneider-Bröskamp C, Enzinger N (2022) Fusion welding of ultra-high strength structural steels – a review. J Manuf Process 82:203–229. https://doi.org/10.1016/j.jmapro.2022.07.049